$TiAg_x$ thin films for lower limb prosthesis pressure sensors: effect of composition and structural changes in the electrical and thermal response of the films

C. Lopes[1], P. Pedrosa[1,2,3], F. Macedo[1], E. Alves[4], N.P. Barradas[4], N. Martin[5], C. Fonseca[2,3], F. Vaz[1*]

[1]Centro de Física, Universidade do Minho, 4710-057 Braga, Portugal

[2]Universidade do Porto, Faculdade de Engenharia, Departamento de Engenharia Metalúrgica e de Materiais, Rua Roberto Frias, s/n, 4200-465 Porto, Portugal

[3]SEG-CEMUC – Department of Mechanical Engineering, University of Coimbra, Portugal

[4]Instituto Tecnológico Nuclear, Dept. Física, E.N. 10, 2686-953 Sacavém, Portugal

[5]Laboratoire de Microanalyse des Surfaces, ENSMM, 26 Chemin de l'Epitaphe, 25000 Besançon Cedex, France

ABSTRACT

$TiAg_x$ thin films were deposited by PVD, onto silicon, glass and polished high-speed steel substrates by DC magnetron sputtering from a pure Ti target with different amounts of Ag pellets, one with, in a wide range of compositions ($0 < x < 0.30$). Ag/Ti ratio will play a crucial rule in the microstructure and morphology of the coatings evidenced in the principal functional properties. For Ag/Ti ratios bellow 0.003, $TiAg_x$ films have similar behaviours to titanium, above this critical value, probably new chemical bonds are established, new structures formed, smooth surfaces appear and significant changes in electrical behaviour could be seen.

...TO COMPLETE

*To whom all correspondence should be sent (fvaz@fisica.uminho.pt)

Keywords: Sputtered films; Sensors, RBS; Electrical Resistivity

1.INTRODUCTION

There are several types of trauma or disease that could progress to a limb amputation, prosthetic devices were than required to replace, part or the entire limb, after the amputation, which according to the EU Directive (42/93/EC) are custom made medical devices, intended to use to compensate for impairments and mobility limitation, allowing a similar to counter lateral, comfortable and safe gait to the amputee. The results of the non-adequate fit of the prosthesis are poor static and dynamic weight support, gait deviations and non-efficient gait. As a consequence, in most cases, there is an overload of the non-amputated side and high-energy consumption. In extreme situations the amputee stops using the device. The production of the prosthesis, and its fit to the amputee, implies alignment of the socket and structure, referring to defined parameters. These assessments are done using qualitative methods, which are not reliable and are based on the experience of the physiatrist. To find a reference…

Starting with this need of having quantitative and reliable information on the suitability of a given prosthesis, different approaches have been carried out to monitor the efforts or pressure fields that are developed all over the contact surface between the patient and its prosthesis. In order to have this pressure maps and thus optimize, not only the shape but also the alignment of the socket, emerges the current work which intends to develop a sensors network device able to monitor the pressure fields at the prosthesis/limb interface, especially artificial lower limbs. The idealization of such a sensors network device obeyed some basic criteria like i) a linear response with the pressure (high sensibility to the pressure); ii) low sensitivity to temperature, material composition and manufacturing technique; and, in

addition, iii) no phase transitions should be found at the operation temperature [1]. Therefore and given its properties (resistant, high flexibility, low density, lightweight, low mechanical impedance) [2, 3] the pruposed sensor array, is being developed and implemented from poli(vinylidene fluoride)-PVDF given its remarkable piezoelectric (sensitive to dynamic pressure fields) and piezoresistive (measure static and dynamic deformations) properties [4] that should provide a good response to measure the mechanical pressures for low and high magnitude carried out by the amputee in the limb prosthesis [1, 4-9].

Anyway, beyond the specific nature and characteristics of the chosen base smart polymeric sensing material (PVDF), there is still the need of its surface functionalization, namely in terms of electric contact. For this, the present approach consists on the use of a magnetron sputtered conductive thin layer. The primordial purpose of this thin layer is to detect, amplify and linearize the strain-induced electric charge or the current produced by the reversible mechanical deformation in the polymeric substrate.

Taking into account the main requirements of the targeted application, the selected layer system should reveal relatively high corrosion and wear resistance, high conductivity and high elasticity (deformation resistance) and, additionally, a good chemical, thermal and mechanical stability. In general, for metallic materials the changes in resistance are linear with strain, and for this reason, they are convenient for pressure and force sensors [10]. Furthermore, the coated polymers will be subjected to mechanical and electrical solicitations and physical contact with human stamp that can cause degradation of the coating and therefore can affect its functional performance. Given the features of the individual elements, the Ti-Ag system was selected. The use of titanium relies on its biocompatibility with human tissues, corrosion resistance, strength and elasticity and excellent thermal and chemical stability [11, 12]. Likewise, and as is well known, silver exhibits a high electrical conductivity, is quite soft and ductile and is a powerful antibacterial component, when

implanted on the material surfaces can exhibit well-effective antibacterial characteristics preventing the formation of bacteria biofilm that could cause inflammation and infection [13-16]. Thus, the addition of silver is expected to be able to tailor the films' flexibility and electrical response, aiming at the same time to give an extra input in terms of biocompatibility due to its bactericide effect.

Taking all this into account, the purpose of the present paper is study the influence of silver additions on the structural and morphological changes of Ti-Ag nanocomposite thin films, and their influence in the electrical and thermal response of the films.

2. EXPERIMENTAL DETAILS

Thin films of $TiAg_x$ have been deposited onto mechanically polished high-speed steel (AISI M2), stainless steel (AISI 316) (conductive substrates), glass and single crystal silicon ((100) orientation) substrates, by reactive DC magnetron sputtering. The depositions were carried out in a pure argon atmosphere, in a laboratory-sized deposition system.

The substrates were ultrasonically cleaned in ethanol before introducing them into the reactor. The films were prepared with the substrate holder positioned at 70 mm from the target, using a DC current density of 100 $A.m^{-2}$ on the titanium target ($200\times100\times6$ mm^3, 99.96 at. % purity), containing different amounts of Ag pellets (with an area of about 64 mm^2), disposed in the preferential eroded zone in order to adjust the variation of silver concentration in the coatings. The total area occupied by the Ag pellets ranged from approximately 1.3×10^{-1} to 8.3 cm^2. The base pressure was below to $4.0x10^{-4}$ Pa, while the Ar pressure during deposition was roughly constant at about 0.3 Pa. The coatings were grown, in rotation mode (7 rpm), without bias voltage, and at a temperature close to 100 ºC.

The atomic composition of the as-deposited samples was measured by Rutherford Backscattering Spectroscopy (RBS) using 1.9 or 2 MeV with ^4He at an angle of incidence 0º

in one small (RBS) chamber. Three detectors were used, one standard located at 140º, and two pin-diode detectors located symmetrical each other, both at 165º. Composition profiles for the as-deposited samples were determined using the software NDF [17]. The error in the Ag concentrations is around 0.02 at.% for the low concentrations.

The structure and phase distribution of the coatings were accessed by X-ray diffraction (XRD), using a conventional Philips PW 1710 diffractometer, operating with Cu K_α radiation, in a Bragg-Brentano configuration. The XRD patterns were deconvoluted and fitted with a Voigt function to determine the structural characteristics of the films, such as the peak position (2θ) and the full width at half maximum (FWHM). Morphological features of the samples were probed by scanning electron microscopy (SEM), carried out in FEI Quanta 400FEG ESEM operating at 15 keV. The films electrical resistivity was measures using the four-probe Van der Pauw's method [18].

Experimetal things about thermal

3. RESULTS AND DISCUSSION

3.1. Discharge characteristics: target potential and deposition rates

Ti-Ag thin films were prepared with similar deposition parameters; nonetheless different discharge voltage and different rates of growth were noticed. Figure 1 shows the evolution of these two characteristics as a function of the area of the Ag pellets placed on the target.

According to the evolution of the discharge voltage during the depositions (Fig.1a), two zones can be identified. In the first one – Zone I, small areas of Ag were exposed and the target potential presented a tenuous decline, with voltage values decreasing from approximately 332 to 322 V, close to value of Ti reference thin film. For the second zone, significant amounts of Ag were used, which resulted in an almost linear increase of the target potential, varying from about 319 to approximately 357 V.

Magnetron sputtering is a complex process, depending on many parameters that are commonly strongly correlated. Important parameters like the target condition, the magnetron configuration, electrical power and the discharge gas [19, 20], are commonly pointed as being crucial to explain its variation. For the present work, the target potential seems to be largely influenced by the composition of the target and by the processes that are occurring during sputtering, which means a strong influence of the plasma characteristics.

The discharge voltage measured during magnetron sputtering, at constant current and sputter pressure (as in this work), is inversely proportional to the ion induced secondary electron emission (ISEE) coefficient of the target material [21], in agreement with equation (1) proposed by Thornton [20]:

$$V_{min} = \frac{W_0}{\gamma_{ISEE} E \varepsilon_i \varepsilon_e} \quad (1)$$

with W_0 representing the effective ionisation energy (about 30 eV for Ar^+) [22], ε_i the ion collection efficiency, ε_e the fraction of the maximum number of ions (for magnetron sputtering ε_i and ε_e are close to unity) E the effective gas ionization probability and γ_{ISEE} the ion induced secondary electron emission coefficient. Based on the empirical relations and measured for the γ_{ISEE} coefficient published by several authors; Depla et al. [19, 20], found an averaged value for several materials; in this particular case the highlights goes to the silver and titanium: γ_{ISEE} (Ag) = 0.110 that is less than γ_{ISEE} (Ti) = 0.114. So an increase in the number of Ag pellets leads to a lower area of Ti exposed, which results in higher values of target potential, since it is inversely proportional to the γ_{ISEE} of the target material. This may explain the behaviour observed for the films prepared within zone II, while the effect of adding small amounts of Ag pellets on Ti target surface could contribute in some way to a higher ionization probability (Ep), maybe due the high sputtering yield of the silver, that might results in a minimum target potential (V_{min}), since V_{min}. is inversely proportional to

E_p.[23] which explains the small decrease of the target potential observed in the films prepared within zone I.

Contrarily to the simple two-fold variation of the target voltage and regarding the influence of Ag pellets in the average thickness per deposition time, (Fig 1b) shows that the deposition rate decreases gradually. However, a closer look reveals that for Ag exposed areas below 1.3 cm^2, the deposition rate is practically constant, varying only slightly between 1.6 and 1.7 μm/h, which may induce a similar chemical and physical behavior of this set of samples. In contrast, $TiAg_x$ thin films prepared with larger amounts of Ag in the target, present a clear tendency for a systematic decrease of the deposition rate, associated to the previous mentioned increase of the target potential.

In terms of the basic mechanisms that may explain this kind of behaviour, one must keep in mind that puttering process of atoms from an elemental target is uniform, since all atoms have the same sputtering yield, but, on the contrary, sputtering of multicomponent targets depends greatly of the individual sputtering yields, of their different masses and of their interactions as a compound. The main effect in the sputtering of multicomponent targets is that the different components are generally in different phases and often with different crystal structure and therefore not sputtered in proportion to their areal concentration on the surface. This effect is called preferential sputtering and was discussed by several authors [20, 21, 24-26]. N Bibic et al. [25], for instance, concluded that sputtering yield of Ag in a AgCu alloy decreases considerably comparatively with a single silver phase, while K. W Pierson et al. [26] reported to a “shadow effect” during the deposition. For these authors, the sputtering yield decreases due to the development of the roughened surface topography. These authors claimed that the sputtered flux was directed toward other nearby features and material redeposit, resulting in a decrease of mass loss that in tum lowers the sputtering yields. All this

statements are in agreement with the gradually decrease of deposition rate, where the high known value of Ag sputtering yield is masked by the composed target effect.

3.2. Deposition Rate and Composition of the as-deposited samples

Fig. 2 shows the chemical composition of the prepared coatings, obtained by RBS spectra analysis, as a function of the total area of Ag exposed on the target surface. The existence of the two distinct groups of samples becomes clear again. In the first group, Ti is the main component (samples were prepared with very small areas of Ag was in the target - below 1.3 cm^2), with an atomic percent close to 99 at.% - a Ti rich zone. For samples prepared within Zone II, the amounts of Ag pellets placed in the target were increased significantly (the area of Ag exposed in the preferential eroded zone increased from 1.9 to 8.3 cm^2) and its content increased also significantly from 5.6 at.% to about 26.5 at%, while Ti content decreased from 94.4 at.% to about 71 at.%. Since Ti and Ag display an opposite trend, the Ag/Ti ratio will be used hereafter to label the samples and to discuss how the changes observed in structural and morphological characterization will affect the functional properties of the samples.

3.3. Structural and Morphological characterization

The structural characterization carried out by XRD, Fig. 3, evidences once again the two clear distinct zones. For the first one of films, where Ti was identified as the major component, the coatings are polycrystalline and exhibit the typical closed packed hexagonal (hcp) structure of Ti, with a preferential (002) growth orientation. However with the Ag addition, Ti epitaxial growth can be clearly observed, and for Ag/Ti ratios above 0.03 the preferred growth happens to be in (011) orientation (ICSD#181718 database). Moreover, XRD diffraction pattern reveal a slight shift in the diffraction angles toward higher values, indicating a lattice distortion for smaller lattice parameters, suggesting some possible vacant

positions of Ti in the hcp structure, probably because Ti atoms are establishing intermetallic bonds with the few Ag atoms that arrived at the substrate surface, since the standard enthalpies of formation of AgTi compounds are favorable [27]. Since Ag atoms exhibit a higher radius than Ti, the substitution of Ti by Ag may not be further considered [28]. At the same time, there are no clear evidences of the presence of a silver phase for this low Ag content zone. Anyway, one must keep in mind that the absence of Ag peaks may not be a direct indication of a Ag phase absence, because it may exist in an amorphous state or the size of the Ag grains and quantity are so small that their diffraction intensity is below the detection limit of the diffractometer [29].

With increasing Ag content, Ag/Ti ratios above 0.12 (Zone II), additional diffraction patterns can be seen (2θ at 37.9º; 44.1º and 64.2º), but their indexing is quite difficult to carry out since they may correspond to different phases according to ICSD database; Ti_2Ag (card nº 605935) TiAg (card nº 605934) or Ag (card nº 181730). The angular positions are rather similar, which does not allow an accurate identification. This set of results leads to the conclusion that there may exist a Ti phase with one of the three Ag phases, or even a mixture of all or two of them [27, 30-32]. Anyway, with the increase of the silver content, the angular position that are observed, compared with the diffraction patterns of the pure Ag film, seem to indicate that an Ag phase (fcc) may prevail over the first.

With growing Ag additions, an increase of the full width at half maximum (FWHM) is noticeable, and the well-defined Ti crystal structure from Zone I, becomes increasingly amorphous in Zone II. There can be several reasons for this progressive amorphization, where the increasing number of Ag defects in the Ti hcp structure due to its incorporation as substitutional or interstitial atoms might be two of the most important ones. The low mobility of the adatoms due to relatively low deposition temperatures, associated with the absence of ion bombardment would certainly facilitate these Ag incorporations in the Ti lattice. This

incorporation would lead to cumulative local lattice disorder, and thus a progressive amorphization of the Ti phase [28].

In order to have some extra input regarding the possible changes in phase formation, the Ti-Ag phase diagram [27], shows that at low Ag concentrations, < 3 at.%, a solid solution of Ag in αTi could be formed, while at higher concentrations a binary phase mixture of αTi and Ti_2Ag, is thermodynamic more favorable, and might be present in the solid state [27, 33]. Although equilibrium phase diagram suggests that for the Ag/Ti atomic ratios obtained in this wok the metallic Ag cannot precipitate, the unfavorable conditions used in this work (no bias and relatively low temperatures) limited the mobility of the adatoms at the growing film, which may give rise to local thermal spikes, leading to a thermodynamic non-equilibrium condition. These non-equilibrium conditions could explain the precipitation of metallic Ag particles, coexisting with TiAg and Ti_2Ag solid solution [34]. This would induce a mixture of Ag phases, which the difractograms in Fig. 3 can actually represent.

To get even further insights, optical measurements might be also of some importance. Some authors showed that UV–visible reflectance measurements are a powerful method for detecting the occurrence of metallic Ag nanograins [35]. In fact, according to the work of Catrin et al., metallic Ag exhibit a characteristic absorption band at 320 nm and reflectance values higher than 95% in the visible region [36], when deposited at room temperature. Figure 4 shows the reflectance measurements in the visible region for the set of $TiAg_x$ coatings prepared within the frame of the present work. Contrarily to what would be expected, the results plotted in Fig. 4 seem to indicate that the Ag atoms are probably not segregated into a metallic phase, since no absorption band is clearly detected in the spectra.

Beyond a change in the structural features of the films with the increase of the Ag content, there is also a change in terms of the microstructure of $TiAg_x$ thin films, which again will have an effect on the physical properties of the films. Figure 6 shows SEM plan view and

cross-section images, denoting the effect of the increase of the Ag content in the evolution of the films microstructure.

In Zone I, the coatings displayed the typical Ti morphology structure, with the formation of three-dimensional hexagonal grain features at the surface (Fig. 5a1, b1, c1), and a characteristic columnar-like growth (Fig. 5a2, b2 and c2), which is expectable given the low Ag content. Anyway, it is also to note that that the Ag addition, even in small amounts, promotes some clear reduction of the surface granularity, maintain though the columnar structure.

With the increase of the Ag content, Zone II, the characteristic hexagonal grain feature of Ti rich thin films at the surface vanishes. The samples from this zone develop smoother surfaces, with fine and denser microstructures. For the samples with the highest Ag/Ti atomic ratio (Fig. 5e1 and e2), brighter spots can be identified at the surface, which are probably from Ag or TiAg clusters segregated from the Ti hexagonal grain boundaries.

3.4. Electrical and Thermal Characterization

Electrical resistivity of metallic systems represents a property sensitive to their electronic structure, availability of charge carriers in the system. Charge carriers resistance is caused by the scattering of electrons due to disturbances in the crystal structure such as solute elements, impurities, grain boundaries, dislocations, vacancies etc. [37]. The total resistivity, at a specific temperature, is the result of all the various scattering processes, that was simplified by Matthiessen's rule, where total resistivity is expressed by the sum of all the calculated terms [38]:

$$\rho_{tot} = \rho_0 + \rho_{ph} + \rho_{mag}$$

where the subscripts denote the residual resistivity (0), the resistivity owing to phonon scattering (ph) and the resistivity owing to spin-dependent scattering (magnetic scattering processes, mag) [38].

The effect of the variable ‘‘impurity’’ scattering is particularly evident for pseudo-binary systems, in agreement with the so-called Nordheim's rule [37, 38]. For this specifically cases the dependence of residual resistivity (ρ_0), on a single solute is expressed as:

$$\rho_0(x) = Ax\ (1 - x)$$

where x is the concentration of the solute and A is a constant which depends on the base metal and solute. The value of A increases with valence, atomic size or other differences between the solvent and solute

In order to study the electrical properties of $TiAg_x$ system, electrical resistivity measurements at room temperature were carried out, and the obtained results (Fig. 6) confirm the evidence of two distinctly electrical behaviours, as in the previous results. The plot of Fig. 7 indicates that for small Ag contents (less than 6 at.%), the resistivity values of the $TiAg_x$ films approaches that of bulk Ti (around 43 μΩ·cm (M.E. Day 1995)). For the values obtained in this first zone (Zone I), and according to Nordheim’s rule, Ag atoms could play the role of solute impurity in Ti solvent structure and a resistivity increase, relatively to Ti thin film, is to be expected due the probability of scattered carriers by impurities. However, and taking into account the well known influence of the grain size in the films electrical behavior, Fig. 7 shows the evolution of the films grain size as a function of the Ag content. From the observation of this figure, its noticeable a sharp decrease of the grain size from 22 nm to 12 nm within the films from zone I. This significant decrease of grain size would, in a first approximation, give rise to an increase in the resistivity due to the increase of grain boundaries scattering. Anyway, the results obtained for the films within this first zone are somewhat contradictory since there seems to be an approximately constant value of resistivity

for all samples. One of the reasons for this behaviour might be related with the good electrical conduction properties of Ag that simultaneously plays a dual role in the Ti structure: impurity and charge carrier, and thus "smoothening" the effect of the grain size reduction and the probable increase of resistivity that it commonly induces.

Still from Fig. 6, it is possible notice a sudden increase of resistivity values when going from zone I to zone II (from about 40 to 70 μΩ·cm), which in fact corresponds to the change in composition results, Fig. 2, but above all, to the exact transition in terms of structural features displayed in Fig. 3. The changes in the crystalline phases that are developed, together with the relatively low values of grain size in the films from zone II (almost constant at about 10 nm) in comparison to those of zone I (above 12 nm), Fig. 7, are certainly parameters that must account for this two-fold behavior. Anyway, and within zone II, it is also to notice a general trend to have a decrease of the electrical resistivity, which could result from the improved crystallinity of the coatings, which can be seen from the increase of the grain size of the grains indexed to the silver phase(s), Fig. 7.

Regarding the thermal characteristics…

4. CONCLUSIONS

ACKNOWLEDGEMENTS

This research is partially sponsored by FEDER funds through the program COMPETE – Programa Operacional Factores de Competitividade and by national funds through FCT – Fundação para a Ciência e a Tecnologia, under the projects PTDC/SAU-ENB/116850/2010 and PTDC/CTM-NAN/112574/2009 and Programa Pessoa 2012/2013 Cooperação Portugal/França, Project nº 27306UA. The authors would also like to acknowledge CEMUP

for SEM analysis. P. Pedrosa acknowledges FCT for the Ph.D. grant SFRH/BD/70035/2010.

BIBLIOGRAPHY

[1] C.O. González-Morán, R. González-Ballesteros, E. Suaste-Gómez, 1st. International Conference on Electrical and Electronics Engineering, (2004) 473-475.

[2] M.S. Inc., (1999) 1-34.

[3] J.E. McKinney, G.T. Davis, M.G. Broadhurst, Journal of Applied Physics, 51 (1980) 1676-1681.

[4] A. Ferrreira, J.G. Rocha, A. Ansón-Casaos, M.T. Martínez, F. Vaz, S. Lanceros-Mendez, Sensors and Actuators A: Physical, 178 (2012) 10-16.

[5] A. Ferreira, P. Cardoso, D. Klosterman, J.A. Covas, F.W.J. van Hattum, F. Vaz, S. Lanceros-Mendez, Smart Materials and Structures, 21 (2012) 075008.

[6] J.M. Gonzalez-Dominguez, A. Ansón-Casaos, M.T. Martinez, A. Ferreira, F. Vaz, S. Lanceros-Méndez, Journal of Intelligent Material Systems and Structures, 23 (2012) 909-917.

[7] A. Ferreira, P. Pedrosa, S. Lanceros-Mendez, A.V. Machado, F. Vaz, Journal of Optoelectronics and Advanced Materials, 12 (2010) 1581-1589.

[8] A. Ferreira, J. Silva, V. Sencadas, J.L.G. Ribelles, S. Lanceros-Méndez, Macromolecular Materials and Engineering, 295 (2010) 523-528.

[9] J.N. Pereira, P. Vieira, A. Ferreira, A.J. Paleo, J.G. Rocha, S. Lanceros-Méndez, Journal of Polymer Research, 19 (2012).

[10] H. Chiriac, M. Urse, F. Rusu, C. Hison, M. Neagu, Sensors and Actuators 76 (1999) 376-380.

[11] V. Chawla, R. Jayaganthan, A.K. Chawla, R. Chandra, Journal of Materials Processing Technology, 209 (2009) 3444-3451.

[12] V. Chawla, R. Jayaganthan, A.K. Chawla, R. Chandra, Materials Chemistry and Physics, 111 (2008) 414-418.

[13] K.-H. Liao, K.-L. Ou, H.-C. Cheng, C.-T. Lin, P.-W. Peng, Applied Surface Science, 256 (2010) 3642-3646.

[14] M.A. Fiori, M.M.d.S. Paula, A.M. Bernardin, H.G. Riella, E. Angioletto, Materials Science and Engineering: C, 29 (2009) 1569-1573.

[15] M.F. Santos, C.M. Oliveira, C.T. Tachinski, M.P. Fernandes, C.T. Pich, E. Angioletto, H.G. Riella, M.A. Fiori, International Journal of Mineral Processing, 100 (2011) 51-53.

[16] R.X. Wang, X.M. Tao, Y. Wang, G.F. Wang, S.M. Shang, Surface and Coatings Technology, 204 (2010) 1206-1210.

[17] N.P. Barradas, C. Jeynes, R.P. Webb, Appl. Phys. Lett., 71 (1997).

[18] V.d. Pauw, Philips Res. Repts, 13 (1958) 1-9.

[19] D. Depla, G. Buyle, J. Haemers, R. De Gryse, Surface and Coatings Technology, 200 (2006) 4329-4338.

[20] D. Depla, J. Haemers, R. De Gryse, Thin Solid Films, 515 (2006) 468-471.

[21] D. Depla, H. Tomaszewski, G. Buyle, R. De Gryse, Surface and Coatings Technology, 201 (2006) 848-854.

[22] M.A. Lieberman, A.J. Lichtenberg, Wiley, New York, (1994) 81.

[23] J. Borges, N. Martin, N.P. Barradas, E. Alves, D. Eyidi, M.F. Beaufort, J.P. Riviere, F. Vaz, L. Marques, Thin Solid Films, 520 (2012) 6709-6717.

[24] S.K. Habib, A. Rizk, I.A. Mousa, Vacuum, 49 (1997) 153-160.

[25] N. BIBIC, I.H. WILSON, M. MILOSAVLJEVIC, D. PERUSKO, Journal of materials Science, 27 (1992) 4945-4948.

[26] K.W. Pierson, J.L. Reeves, T.D. Krueger, C.D. Hawes, C.B. Cooper, Nuclear Instruments and Methods in Physics Research, B 108 (1996) 290-299.

[27] M. Li, C. Li, F. Wang, W. Zhang, Calphad, 29 (2005) 269-275.

[28] J.F. Pierson, D. Horwat, Scripta Materialia, 58 (2008) 568-570.

[29] J.G. Han, H.S. Myung, H.M. Lee, L.R. Shaginyan, Surface and Coatings Technology, 174-175 (2003) 738-743.

[30] X. Wang, F. Prokert, H. Reuther, M.F. Maitz, F. Zhang, Surface and Coatings Technology, 185 (2004) 12-17.

[31] C. Guo, J. Chen, J. Zhou, J. Zhao, L. Wang, Y. Yu, H. Zhou, Applied Surface Science, 257 (2011) 10692-10698.

[32] J.-B. Han, Y.-B. Han, D.-J. Chen, S. Ding, Q.-Q. Wang, Materials Letters, 60 (2006) 467-469.

[33] A. Ewald, S.K. Gluckermann, R. Thull, U. Gbureck, Biomedical engineering online, 5 (2006) 22.

[34] H. Cao, X. Liu, F. Meng, P.K. Chu, Biomaterials, 32 (2011) 693-705.

[35] R. Catrin, D. Horwat, J.F. Pierson, S. Migot, Y. Hu, F. Mücklich, Applied Surface Science, 257 (2011) 5223-5229.

[36] T. Suzuki, Y. Abe, M. Kawamura, K. Sasaki, T. Shouzu, K. Kawamata, Vacuum, 66 (2002) 501-504.

[37] S. Nagarjuna, K. Balasubramanian, D.S. Sarma, Materials Science and Engineering, A225 (1997) 118-124.

[38] E. Gratz, Encyclopedia of Materials: Science and Technology (Second Edition), (2001) 4152-4158.

Figure captions

Fig. 1. Discharge characteristics of $TiAg_x$ thin films: evolution of the deposition rate **(a)** and the target potential **(b)** with increasing Ag area exposed in the target.

Figure 1

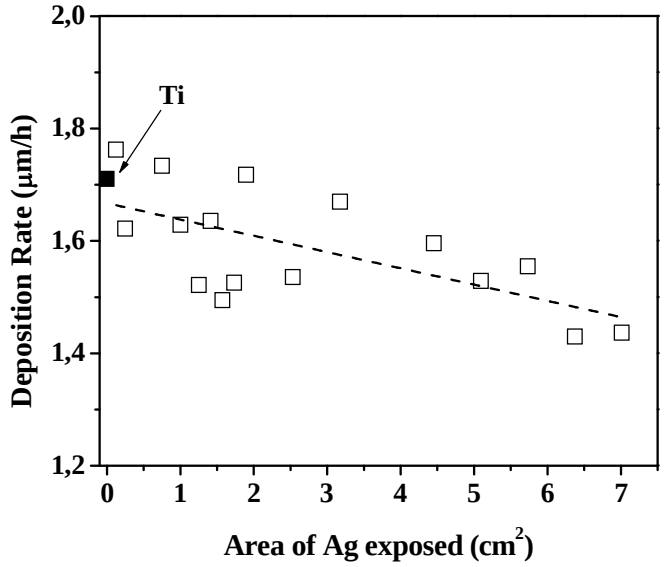
Deposition Rate (µm/h)
2,0
1,8
1,6
1,4
1,2
Ti
0
1
2
3
4
5
6
7
Area of Ag exposed (cm2)

a)

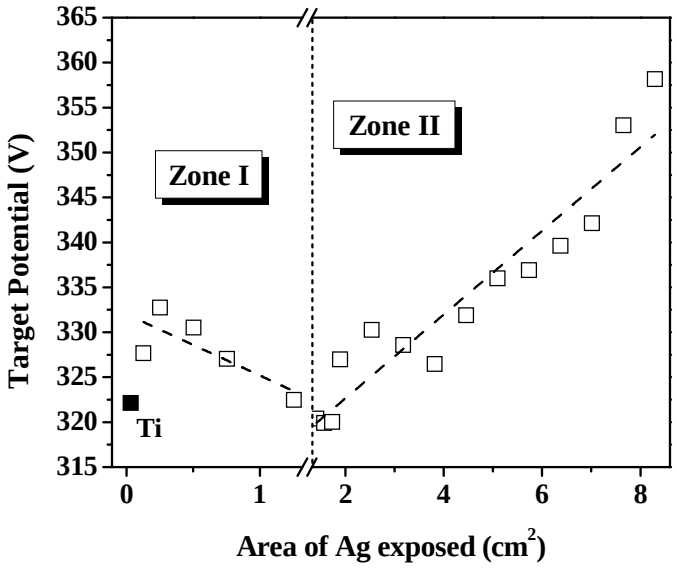
Target Potential (V)
365
360
355
350
345
340
335
330
325
320
315
Zone I
Zone II
Ti
0
1
2
4
6
8
Area of Ag exposed (cm2)

b)

Figure 2

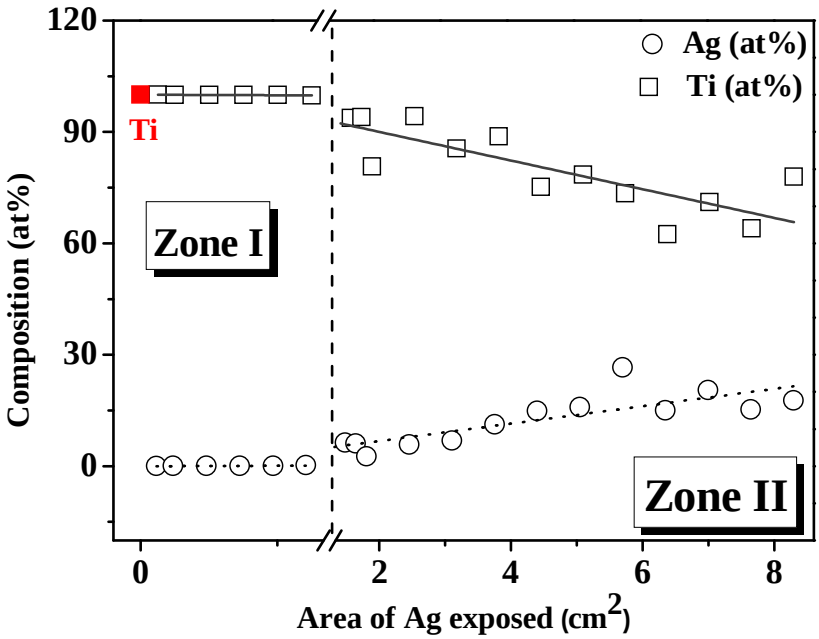
120
90
60
30
0
Composition (at%)
Ag (at%)
Ti (at%)
Ti
Zone I
Zone II
0
2
4
6
8
Area of Ag exposed (cm2)

Figure 3

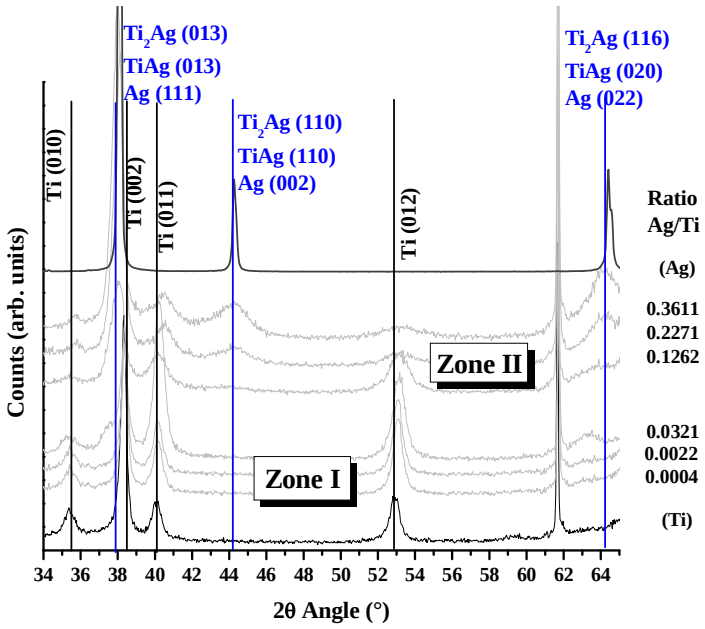
Ti2Ag (013)
TiAg (013)
Ag (111)
Ti2Ag (110)
TiAg (110)
Ag (002)
Ti2Ag (116)
TiAg (020)
Ag (022)
Ti (010)
Ti (002)
Ti (011)
Ti (012)
Zone I
Zone II
Ratio Ag/Ti
(Ag)
0.3611
0.2271
0.1262
0.0321
0.0022
0.0004
(Ti)
Counts (arb. units)
34 36 38 40 42 44 46 48 50 52 54 56 58 60 62 64
2θ Angle (°)

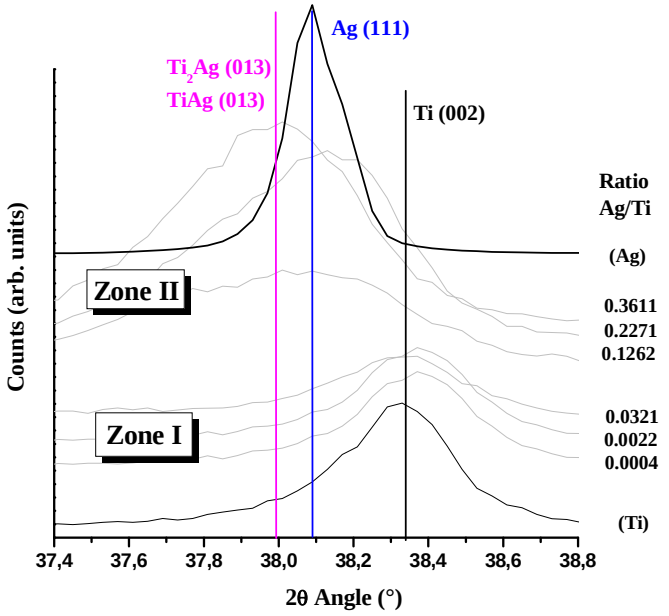
Ag (111)
Ti2Ag (013)
TiAg (013)
Ti (002)
Zone II
Zone I
Ratio Ag/Ti
(Ag)
0.3611
0.2271
0.1262
0.0321
0.0022
0.0004
(Ti)
Counts (arb. units)
37,4 37,6 37,8 38,0 38,2 38,4 38,6 38,8
2θ Angle (°)

Figure 4

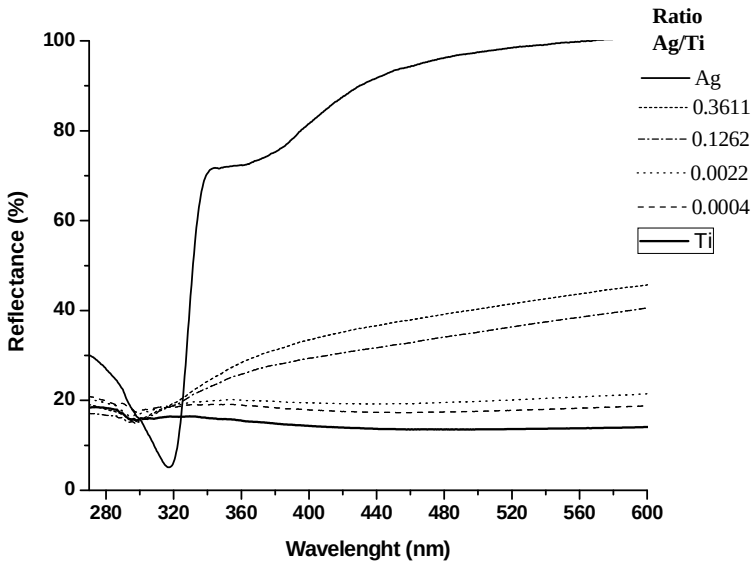
Ratio
Ag/Ti
Ag
0.3611
0.1262
0.0022
0.0004
Ti
Reflectance (%)
Wavelenght (nm)
0
20
40
60
80
100
280
320
360
400
440
480
520
560
600

Figure 5

Zone I

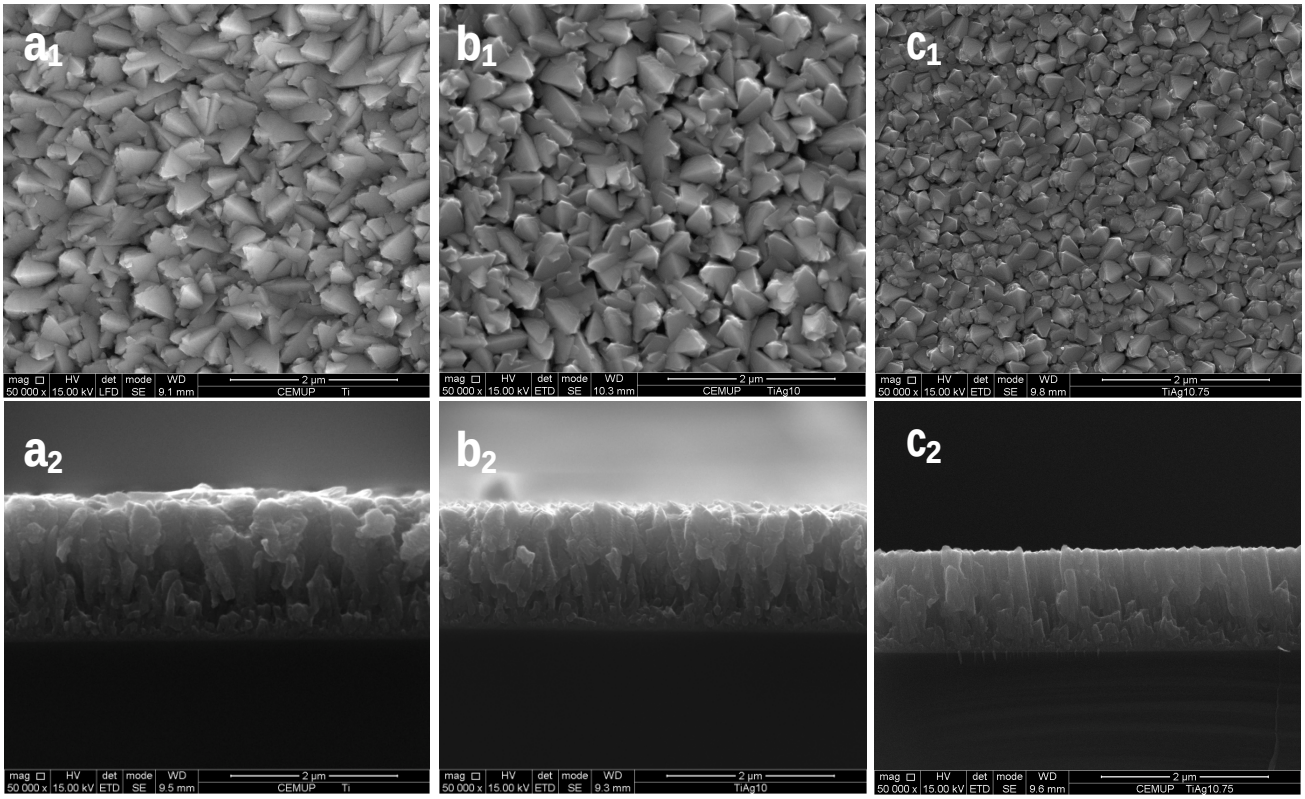

Zone II

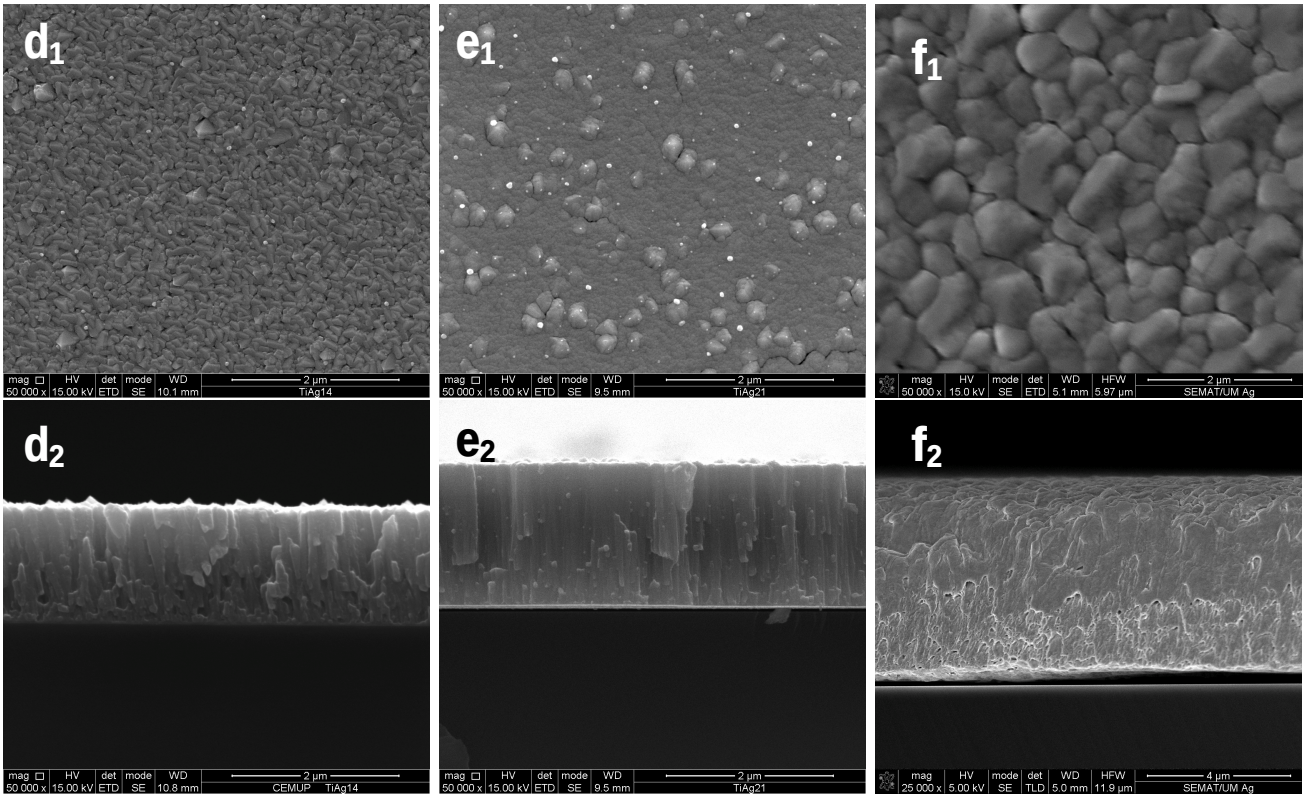

Figure 6

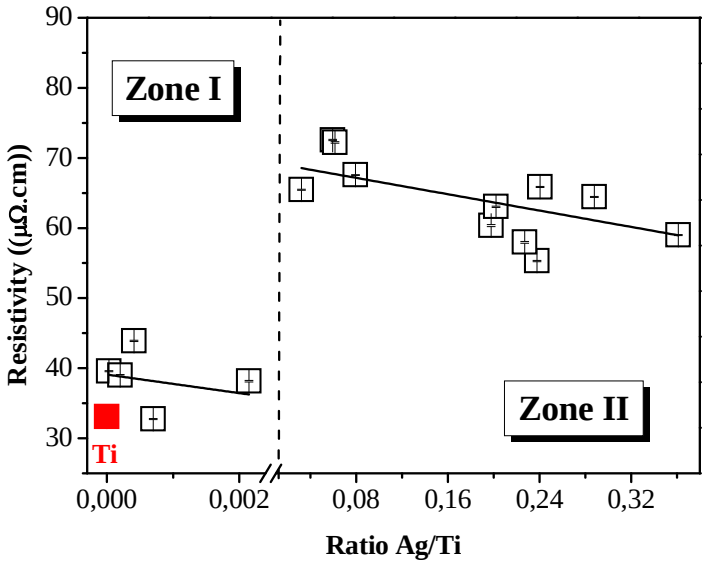
Zone I
Zone II
Ti
Resistivity ((μΩ.cm))
Ratio Ag/Ti
90
80
70
60
50
40
30
0,000
0,002
0,08
0,16
0,24
0,32

Figure 7

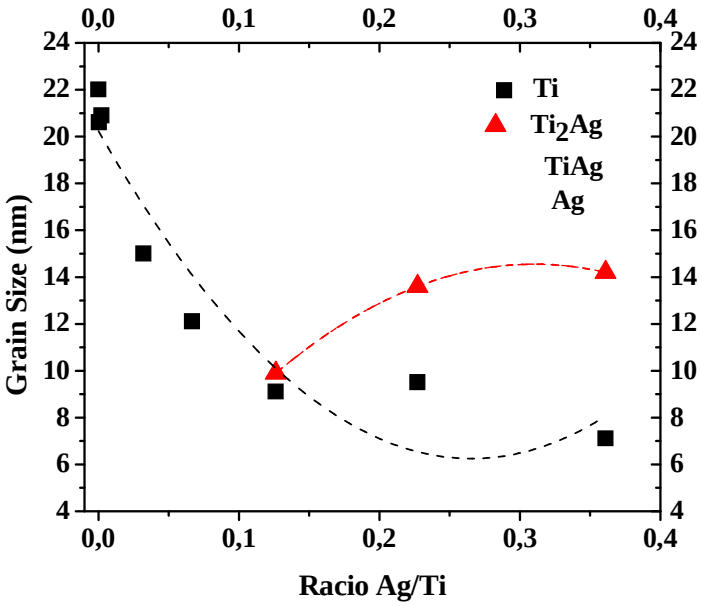
Grain Size (nm)
Racio Ag/Ti
Ti
Ti2Ag
TiAg
Ag
0,0
0,1
0,2
0,3
0,4
4
6
8
10
12
14
16
18
20
22
24